PERGAMON

Engineering Fracture Mechanics 61 (1998) 471–485

Engineering Fracture Mechanics

Effect of elastic mismatch in intersonic crack propagation along a bimaterial interface

W. Wang[a], Y. Huang[b,*], A.J. Rosakis[c], C. Liu[d]

[a]*Department of Mechanical Engineering–Engineering Mechanics, Michigan Technological University, Houghton, MI 49931, USA*

[b]*Department of Mechanical and Industrial Engineering, University of Illinois at Urbana-Champaign, Urbana, IL 61801, USA*

[c]*Graduate Aeronautical Laboratories, California Institute of Technology, Pasadena, CA 91125, USA*

[d]*MST-8, MS-G755, Materials Science and Technology Division, Los Alamos National Laboratories, Los Alamos, NM 87545, USA*

Received 5 May 1998; received in revised form 21 September 1998; accepted 25 September 1998

Abstract

Recent experiments showed that the speed of a crack tip propagating along a bimaterial interface can exceed the shear wave speed of the more compliant constituent in the bimaterial. This experimental observation has motivated analytical and numerical investigation on fast crack growth. Among these investigations, Huang et al. obtained a simple, analytic full-field solution for an elastic/rigid bimaterial with crack-face contact. Although this solution compares quite favorably with all available experimental data, it is not clear which bimaterial can be approximated by the elastic/rigid model. In this paper, we use the method of analytical continuation to obtain the asymptotic stress fields near the crack tip and near the trailing end of the contact zone. It is established that the elastic/rigid model is an excellent approximation to all bimaterials that have been used in fast crack growth experiments. Therefore, the simple, analytic solution of elastic/rigid model provides a useful means for analyzing experimental fringe patterns and data. It is shown that, as the elastic mismatch decreases, the elastic/rigid model may become invalid. © 1998 Elsevier Science Ltd. All rights reserved.

Keywords: Elastic mismatch; Intersonic crack propagation; Interface

* Corresponding author. Tel.: +1-217-265-5072; fax: +1-217-244-6534; e-mail: huang9@uiuc.edu.

0013-7944/98/$ - see front matter © 1998 Published by Elsevier Science Ltd. All rights reserved.
PII: S0013-7944(98)00089-7

1. Introduction

Recent experimental studies of Tippur and Rosakis [9], Liu et al. [6], Lambros and Rosakis [5] showed some surprising phenomena in dynamic interfacial fracture. For a PMMA/Steel bimaterial, the interfacial crack tip speed was observed to rapidly approach and exceed not only the Rayleigh wave speed, but also the shear wave speed of PMMA. This crack tip speed certainly exceeds Atkinson's [1] claim of terminal speed of an interfacial crack, which is the lower of the two Rayleigh wave speeds of constituents in a bimaterial. Motivated by the earliest of these experimental observations, Yang et al. [11] conducted a steady-state asymptotic analysis of subsonic interfacial crack growth in the bimaterial, and established that, unlike crack growth in homogeneous materials, the crack tip energy release rate remains bounded as the crack tip speed approaches the lower Rayleigh wave speed of the bimaterial. As a result, it was shown to be theoretically possible for an interfacial crack tip to exceed the lower Rayleigh wave speed, which, in fact, was consistent with experimental results.

Motivated by these new experimental observations, Liu et al. [7], Yu and Yang [12], Huang et al. [3] investigated the near-tip fields around an intersonically propagating interfacial crack tip whose crack faces remain traction-free. They showed that stresses are singular not only at the crack tip, but also on an entire ray propagating with the crack tip. This ray, similar to a shock wave in aerodynamics, represents a line of strong discontinuity and has been observed in a series of experimental studies [5, 6, 8]. These analytical studies, however, have not taken into account the effect of large crack face contact zone that exists behind the crack tip observed in experiments using optical method of CGS (coherent gradient sensing) [5] or photoelasticity [8]. This finite contact zone is on the order of millimeters [5, 8] and is too large to be neglected. Crack face contact and the existence of shock wave type stress discontinuities traveling with the crack tip have also been observed in the numerical simulations of Xu and Needleman [10].

Finite contact behind the crack tip propagating intersonically raises the possibility of two shock waves being generated at the moving crack tip and at the trailing end of the contact zone. Indeed, the most recent experimental observations based on photoelasticity clearly show the existence of two such shock waves that are equally inclined to the interface and propagate with the same speed for substantial time periods throughout the experiments [8]. Motivated by the aforementioned experimental and numerical observations, Huang et al. [4] investigated the stress field around a crack tip propagating intersonically along the interface between an elastic medium and a rigid substrate. The analysis predicted successfully the essential features observed in CGS and photoelasticity experiments, including two distinct velocity dependent singularities at the crack tip and at the trailing end of the contact region, as well as the appearance of two distinct shock waves emanating from these two points. The reason for Huang et al. [4] to study the elastic/rigid bimaterial is that, in Lambros and Rosakis' [5] experiments, the elastic moduli of steel are almost two orders of magnitudes higher than those of PMMA. Moreover, an analytic full-field solution can be obtained for the elastic/rigid bimaterial, therefore it provides a simple and useful means for analyzing experimentally obtained fringe patterns and data. However, it should be pointed out the mass density of steel is almost one order of magnitude higher than that of PMMA such that the mismatch in shear wave speeds between PMMA and steel are much smaller than the mismatch in elastic moduli.

Further studies are needed to evaluate whether the elastic/rigid model is a good approximation to an elastic/elastic bimaterial.

This paper presents an investigation of the asymptotic stress fields near an intersonically propagating interfacial crack tip as well as near the trailing end of the contact zone for an elastic/elastic bimaterial with crack face contact. It compares with the elastic/rigid model [4] in order to determine the range of mismatch in elastic moduli and mass densities whereby the elastic/rigid model is a good approximation. Section 2 provides the general structure of the solution in each constituent of the bimaterial, while the method of analytic continuation is used in Sections 3 and 4 to obtain the asymptotic fields near the crack tip and near the trailing end of the contact zone, respectively.

2. Modeling of intersonic crack growth along a bimaterial interface

As shown in Fig. 1, the interface between the two elastic solids lies in the x_1 axis. It is assumed that the upper solid (indicated by superscript "1") is more compliant than the lower solid (indicated by superscript "2"). The crack tip propagates in the positive x_1 direction at a speed v, such that

$$c_s^{(1)} < v < \min\left[c_s^{(2)}, c_l^{(1)}\right] \tag{1}$$

for intersonic crack growth, where $c_s^{(i)} = \sqrt{\mu^{(i)}/\rho^{(i)}}$ and $c_l^{(i)} = \sqrt{(\kappa^{(i)}+1)/(\kappa^{(i)}-1)c_s^{(i)}}$ (i = 1, 2) are the shear and longitudinal wave speeds of the ith constituent in the bimaterial, respectively, $\mu^{(i)}$ is the elastic shear modulus, $\rho^{(i)}$ is the mass density, $\kappa^{(i)} = 3 - 4\nu^{(i)}$ for plane strain and $\kappa^{(i)} = (3 - \nu^{(i)})/(1 + \nu^{(i)})$ for plane stress, and $\nu^{(i)}$ is the Poisson's ratio. The in-plane displacements $u_1^{(i)}$ and $u_2^{(i)}$ (i = 1, 2) in the elastic solids can be expressed by four displacement potentials $\phi^{(i)}$ and $\psi^{(i)}$ (i = 1, 2) as

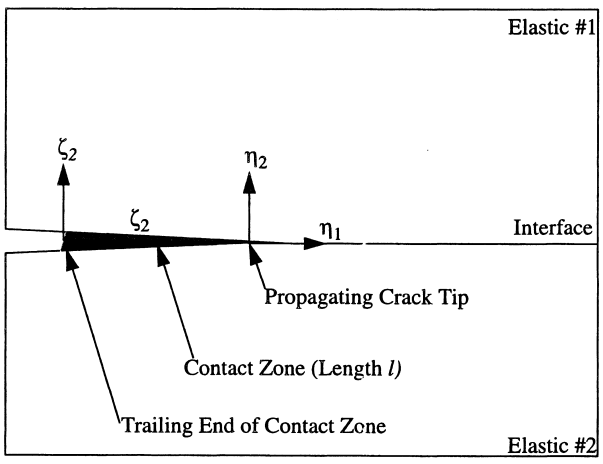

Fig. 1. An interface crack propagating intersonically between two elastic solids. There is a finite contact zone of length l at the interface between the two elastic media, trailing the crack tip.

$$u_1^{(i)}(x_1, x_2, t) = \frac{\partial}{\partial x_1}\phi^{(i)}(x_1, x_2, t) + \frac{\partial}{\partial x_2}\psi^{(i)}(x_1, x_2, t) \tag{2a}$$

$$u_2^{(i)}(x_1, x_2, t) = \frac{\partial}{\partial x_2}\phi^{(i)}(x_1, x_2, t) - \frac{\partial}{\partial x_1}\psi^{(i)}(x_1, x_2, t) \tag{2b}$$

It is assumed that the crack growth is steady-state, and by introducing the moving coordinate $(\eta_1, \eta_2) = (x_1 - \upsilon t, x_2)$, the equation of motion becomes [2]

$$\left.\begin{aligned} \phi_{,11}^{(1)}(\eta_1, \eta_2) + \frac{1}{\alpha_{l1}^2}\phi_{,22}^{(1)}(\eta_1, \eta_2) = 0 \\ \psi_{,11}^{(1)}(\eta_1, \eta_2) - \frac{1}{\hat{\alpha}_{s1}^2}\psi_{,22}^{(1)}(\eta_1, \eta_2) = 0 \end{aligned}\right\} \quad \eta_2 > 0, \tag{3a}$$

and

$$\left.\begin{aligned} \phi_{,11}^{(2)}(\eta_1, \eta_2) + \frac{1}{\alpha_{l2}^2}\phi_{,22}^{(2)}(\eta_1, \eta_2) = 0 \\ \psi_{,11}^{(2)}(\eta_1, \eta_2) + \frac{1}{\alpha_{s2}^2}\psi_{,22}^{(2)}(\eta_1, \eta_2) = 0 \end{aligned}\right\} \quad \eta_2 < 0, \tag{3b}$$

where

$$\alpha_{l1} = \left(1 - \frac{\upsilon^2}{c_l^{(1)2}}\right)^{\frac{1}{2}} \tag{4a}$$

$$\hat{\alpha}_{s1} = \left(\frac{\upsilon^2}{c_s^{(1)2}} - 1\right)^{\frac{1}{2}} \tag{4b}$$

$$\alpha_{l2} = \left(1 - \frac{\upsilon^2}{c_l^{(2)2}}\right)^{\frac{1}{2}} \tag{4c}$$

and

$$\alpha_{s2} = \left(1 - \frac{\upsilon^2}{c_s^{(2)2}}\right)^{\frac{1}{2}} \tag{4d}$$

As discussed in [3], the general solution of Eq. (3) is

$$\left.\begin{aligned} \phi^{(1)}(\eta_1, \eta_2) = \mathrm{Re}\{F_1(z_{l1})\} \\ \psi^{(1)}(\eta_1, \eta_2) = g(\eta_1 + \hat{\alpha}_{s1}\eta_2) \end{aligned}\right\} \quad \eta_2 > 0 \tag{5a}$$

and

$$\left.\begin{aligned}\phi^{(2)}(\eta_1,\eta_2) &= \mathrm{Re}\{F_2(z_{l2})\}\\ \psi^{(2)}(\eta_1,\eta_2) &= \mathrm{Im}\{G_2(z_{s2})\}\end{aligned}\right\}\qquad \eta_2<0 \tag{5b}$$

where $z_{l1}=\eta_1+i\alpha_{l1}\eta_2$, $z_{l2}=\eta_1+i\alpha_{l2}\eta_2$ and $z_{s2}=\eta_1+i\alpha_{s2}\eta_2$, $\mathrm{Re}\{\cdot\}$ and $\mathrm{Im}\{\cdot\}$ stand for the real and imaginary parts of a complex argument, respectively, $F_1(z_{l1})$ is an analytical function of z_{l1} in the upper half plane, $\eta_2\geq 0$, $g(\eta_1+\hat{\alpha}_{s1}\eta_2)$ is a real function of its argument, $F_2(z_{l2})$ and $G_2(z_{s2})$ are analytical functions of their arguments in the lower half plane, $\eta_2<0$. Displacements and stresses can be expressed as

$$\left.\begin{aligned}u_1^{(1)} &= \mathrm{Re}\{F_1'(z_{l1})\}+\hat{\alpha}_{s1}\,g'(\eta_1+\hat{\alpha}_{s1}\,\eta_2)\\ u_2^{(1)} &= -\alpha_{l1}\,\mathrm{Im}\{F_1'(z_{l1})\}-g'(\eta_1+\hat{\alpha}_{s1}\,\eta_2)\end{aligned}\right\}\qquad \eta_2>0 \tag{6a}$$

and

$$\left.\begin{aligned}u_1^{(2)} &= \mathrm{Re}\{F_2'(z_{l2})+\alpha_{s2}\,G_2'(z_{s2})\}\\ u_2^{(2)} &= -\mathrm{Im}\{\alpha_{l2}\,F_2'(z_{l2})+G_2'(z_{s2})\}\end{aligned}\right\}\qquad \eta_2<0 \tag{6b}$$

$$\left.\begin{aligned}\sigma_{11}^{(1)} &= \mu^{(1)}\Big[(1+2\alpha_{l1}^2+\hat{\alpha}_{s1}^2)\,\mathrm{Re}\,\{F_1''(z_{l1})\}+2\hat{\alpha}_{s1}\,g''(\eta_1+\hat{\alpha}_{s1}\eta_2)\Big]\\ \sigma_{22}^{(1)} &= -\mu^{(1)}\Big[(1-\hat{\alpha}_{s1}^2)\,\mathrm{Re}\,\{F_1''(z_{l1})\}+2\hat{\alpha}_{s1}\,g''(\eta_1+\hat{\alpha}_{s1}\eta_2)\Big]\\ \sigma_{12}^{(1)} &= -\mu^{(1)}\Big[2\alpha_{l1}\,\mathrm{Im}\,\{F_1''(z_{l1})\}+(1-\hat{\alpha}_{s1}^2)\,g''(\eta_1+\hat{\alpha}_{s1}\eta_2)\Big]\end{aligned}\right\}\qquad \eta_2>0 \tag{7a}$$

and

$$\left.\begin{aligned}\sigma_{11}^{(2)} &= \mu^{(2)}\mathrm{Re}\left\{(1+2\alpha_{l2}^2-\alpha_{s2}^2)F_2''(z_{l2})+2\alpha_{s2}\,G_2''(z_{s2})\right\}\\ \sigma_{22}^{(2)} &= -\mu^{(2)}\mathrm{Re}\left\{(1+\alpha_{s2}^2)F_2''(z_{l2})+2\alpha_{s2}\,G_2''(z_{s2})\right\}\\ \sigma_{12}^{(2)} &= -\mu^{(2)}\mathrm{Im}\left\{2\alpha_{l2}\,F_2''(z_{l2})+(1+\alpha_{s2}^2)\,G_2''(z_{s2})\right\}\end{aligned}\right\}\qquad \eta_2<0 \tag{7b}$$

Functions F_1, g, F_2 and G_2 are determined by the continuity of displacements and stresses across the interface, the traction-free condition on crack faces, and the contact condition within the contact zone, as discussed in Section 3 for the asymptotic field near the crack tip and Section 4 for that near the trailing end of the contact zone.

3. Asymptotic field near the crack tip

At the interface ($\eta_2=0$, $\eta_1>0$), the continuity of displacements and stresses gives $[u_1]=0$, $[u_2]=0$, $[\sigma_{22}]=0$ and $[\sigma_{12}]=0$, i.e. for $\eta_1>0$,

$$F_1'^{+}(\eta_1)+\bar{F}_1'^{-}(\eta_1)+2\hat{\alpha}_{s1}\,g'(\eta_1) = \bar{F}_2'^{+}(\eta_1)+F_2'^{-}(\eta_1)+\alpha_{s2}\left[\bar{G}_2'^{+}(\eta_1)+G_2'^{-}(\eta_1)\right] \tag{8a}$$

$$\alpha_{l1}\left[F_1'^{+}(\eta_1)-\bar{F}_1'^{-}(\eta_1)\right]+2ig'(\eta_1) = \alpha_{l2}\left[F_2'^{-}(\eta_1)-\bar{F}_2'^{+}(\eta_1)\right]+G_2'^{-}(\eta_1)-\bar{G}_2'^{+}(\eta_1) \tag{8b}$$

$$\frac{\mu^{(1)}}{\mu^{(2)}}\left\{(1-\hat{\alpha}_{s1}^2)\left[F_1''^{+}(\eta_1)+\bar{F}_1''^{-}(\eta_1)\right]+4\hat{\alpha}_{s1}\,g''(\eta_1)\right\} = (1+\alpha_{s2}^2)\left[F_2''^{-}(\eta_1)+\bar{F}_2''^{+}(\eta_1)\right]+2\alpha_{s2}\left[G_2''^{-}(\eta_1)+\bar{G}_2''^{+}(\eta_1)\right] \tag{8c}$$

and

$$\frac{\mu^{(1)}}{\mu^{(2)}}\left\{(1-\hat{\alpha}_{s1}^2)\left[F_1''^{+}(\eta_1)+\bar{F}_1''^{-}(\eta_1)\right]+4\hat{\alpha}_{s1}\,g''(\eta_1)\right\} = 2\alpha_{l2}\left[F_2''^{-}(\eta_1)-\bar{F}_2''^{+}(\eta_1)\right]+(1+\alpha_{s2}^2)\left[G_2''^{-}(\eta_1)-\bar{G}_2''^{+}(\eta_1)\right] \tag{8d}$$

where $\bar{F}_1(z_{l1})=\overline{F_1(\bar{z}_{l1})}$ is an analytic function in the lower half plane of z_{l1}, $\bar{F}_2(z_{l2})=\overline{F_2(\bar{z}_{l2})}$ and $\bar{G}_2(z_{s2})=\overline{G_2(\bar{z}_{s2})}$ are analytical functions in the upper half plane of their corresponding arguments, and superscripts " + " and " − " stand for the limits for $\eta_2\to 0^+$ and $\eta_2\to 0^-$, respectively. By eliminating $g(\eta_1)$, one finds

$$M\begin{bmatrix} F_1''^{+}(\eta_1) \\ \bar{F}_2''^{+}(\eta_1) \\ \bar{G}_2''^{+}(\eta_1) \end{bmatrix} - \bar{M}\begin{bmatrix} \bar{F}_1''^{-}(\eta_1) \\ F_2''^{-}(\eta_1) \\ G_2''^{-}(\eta_1) \end{bmatrix} = 0 \qquad \eta_1>0 \tag{9}$$

where

$$M=\begin{bmatrix} \gamma\left[2\hat{\alpha}_{s1}\alpha_{l1}-i(1-\hat{\alpha}_{s1}^2)\right] & 2\gamma\hat{\alpha}_{s1}\alpha_{l2}+i(1+\alpha_{s2}^2) & 2\gamma\hat{\alpha}_{s1}+2i\alpha_{s2} \\ \gamma\alpha_{l1}(1+\hat{\alpha}_{s1}^2) & \alpha_{l2}\left[2-\gamma(1-\hat{\alpha}_{s1}^2)\right] & 1+\hat{\alpha}_{s2}^2-\gamma(1-\hat{\alpha}_{s1}^2) \\ \hat{\alpha}_{s1}^2\alpha_{l1}-i & \hat{\alpha}_{s1}\alpha_{l2}+i & \hat{\alpha}_{s1}+i\alpha_{s2} \end{bmatrix} \tag{10}$$

and $\gamma=\mu^{(1)}/\mu^{(2)}$. Based on analytical continuation, Eq. (9) defines the following analytic function

$$\left.\begin{aligned} \vec{\theta}'(z) &= M\begin{bmatrix} F_1''(z) \\ \bar{F}_2''(z) \\ \bar{G}_2''(z) \end{bmatrix} \quad \mathrm{Im}(z) \geq 0 \\ \vec{\theta}'(z) &= \bar{M}\begin{bmatrix} \bar{F}_1''(z) \\ F_2''(z) \\ G_2''(z) \end{bmatrix} \quad \mathrm{Im}(z) < 0 \end{aligned}\right\} \tag{11}$$

where $\vec{\theta}'(z)$ is analytic in the entire z-plane, except on the crack face ($\eta_2 = 0$, $\eta_1 < 0$).

Because of the existence of a crack face contact zone behind the crack tip, the normal displacement u_2, the normal stress σ_{22} and shear stress σ_{12} within the contact zone should be continuous, i.e.

$$[u_2] = 0, \quad [\sigma_{22}] = 0, \quad [\sigma_{12}] = 0 \quad \text{for} \quad \eta_1 < 0 \; \eta_2 = 0 \tag{12}$$

They are identical to Eqs. (8b)–(8 d) except that they are imposed on the entire crack face ($\eta_1 < 0$, $\eta_2 = 0$) in the present asymptotic analysis near the crack tip. The additional boundary condition comes from the linear contact model [4], where the shear and normal stresses within the contact zone are related by

$$\sigma_{12} = \lambda\sigma_{22} \quad \eta_1 < 0 \quad \eta_2 = 0 \tag{13}$$

where the contact coefficient of proportionality λ is assumed to depend on bimaterial and bond properties. Eq. (13) can be written, via the expression of stresses in Eq. (7), as

$$\left.\begin{aligned} &2\alpha_{11}\left[F_1''^{+}(\eta_1) - \bar{F}_1''^{-}(\eta_1)\right] + 2i(1-\hat{\alpha}_{s1}^2)\,g''(\eta_1) \\ &\quad = \lambda\left\{i(1-\hat{\alpha}_{s1}^2)\left[F_1''^{+}(\eta_1) + \bar{F}_1''^{-}(\eta_1)\right] + 4\hat{\alpha}_{s1} i g''(\eta_1)\right\} \end{aligned}\right\} \quad \eta_1 < 0 \tag{14}$$

The elimination of $g(\eta_1)$ from Eqs. (8b)–(8 d) and Eq. (14) leads to

$$P\begin{bmatrix} F_1''^{+}(\eta_1) \\ \bar{F}_2''^{+}(\eta_1) \\ \bar{G}_2''^{+}(\eta_1) \end{bmatrix} - \bar{P}\begin{bmatrix} \bar{F}_1''^{-}(\eta_1) \\ F_2''^{-}(\eta_1) \\ G_2''^{-}(\eta_1) \end{bmatrix} = 0 \qquad \eta_1 < 0 \tag{15}$$

where

$$P = \begin{bmatrix} \gamma\left[2\hat{\alpha}_{s1}\alpha_{l1} - i(1-\hat{\alpha}_{s1}^2)\right] & 2\gamma\hat{\alpha}_{s1}\alpha_{l2} + i(1+\alpha_{s2}^2) & 2\gamma\hat{\alpha}_{s1} + 2i\alpha_{s2} \\ \gamma\alpha_{l1}(1+\hat{\alpha}_{s1}^2) & \alpha_{l2}\left[2-\gamma(1-\hat{\alpha}_{s1}^2)\right] & 1+\hat{\alpha}_{s2}^2 - \gamma(1-\hat{\alpha}_{s1}^2) \\ 2\lambda\alpha_{l1}\hat{\alpha}_{s1}^2 + \alpha_{l1}(1+\hat{\alpha}_{s1}^2) - i\lambda(1-\hat{\alpha}_{s1}^2) & \alpha_{l2}\left[2\lambda\hat{\alpha}_{s1} - (1-\hat{\alpha}_{s1}^2)\right] & 2\lambda\hat{\alpha}_{s1} - (1-\hat{\alpha}_{s1}^2) \end{bmatrix} \tag{16}$$

In terms of the analytic function $\boldsymbol{\theta}'(z)$ in Eq. (11), Eq. (15) can be expressed as

$$PM^{-1}\vec{\theta}'^{+}(\eta_1) - \bar{P}\bar{M}^{-1}\vec{\theta}'^{-}(\eta_1) = 0 \qquad \eta_1 < 0 \tag{17}$$

Let λ_1, λ_2 and λ_3 be eigenvalues and $\vec{\boldsymbol{\chi}}_1$, $\vec{\boldsymbol{\chi}}_2$ and $\vec{\boldsymbol{\chi}}_3$ be the corresponding orthogonal eigenvectors for the following auxiliary eigenvalue problem

$$PM^{-1}\vec{\chi} - \lambda\bar{P}\bar{M}^{-1}\vec{\chi} = 0 \tag{18}$$

which can be easily solved by a numerical method. The function $\vec{\boldsymbol{\theta}}'(z)$ can be written in terms of eigenvectors $\vec{\boldsymbol{\chi}}_i$ (i = 1,2,3) as

$$\vec{\theta}'(z) = \theta_1'(z)\vec{\chi}_1 + \theta_2'(z)\vec{\chi}_2 + \theta_3'(z)\vec{\chi}_3 = \left(\vec{\chi}_1, \vec{\chi}_2, \vec{\chi}_3\right)\begin{bmatrix} \theta_1'(z) \\ \theta_2'(z) \\ \theta_3'(z) \end{bmatrix} \tag{19}$$

where $\theta_i'(z)$ (i = 1,2,3) are analytic except at the crack face. The substitution of expansion (19) into Eq. (17) gives

$$\begin{bmatrix} \lambda_1\theta_1'^{+}(\eta_1) - \theta_1'^{-}(\eta_1) \\ \lambda_2\theta_2'^{+}(\eta_1) - \theta_2'^{-}(\eta_1) \\ \lambda_3\theta_3'^{+}(\eta_1) - \theta_3'^{-}(\eta_1) \end{bmatrix} = 0 \qquad \eta_1 < 0 \tag{20}$$

which constitutes three Riemann–Hilbert problems for $\theta_1'(z)$, $\theta_2'(z)$ and $\theta_3'(z)$, respectively. Their general solutions are

$$\theta_j'(z) = A_j(z)/z_z^{q_j} \qquad j = 1, 2, 3 \tag{21}$$

where $A_j(z)$ are analytic in the entire z-plane, and q_j are the powers of stress singularity near the crack tip and are given by

$$q_j = \frac{1}{2\pi i}\ln\lambda_j \qquad j = 1, 2, 3 \tag{22}$$

These powers of stress singularity near the crack tip depend on the crack tip velocity υ, bimaterial properties, as well as the contact coefficient of proportionality λ. In fact, due to crack face contact, the powers of stress singularity are always real such that there is no

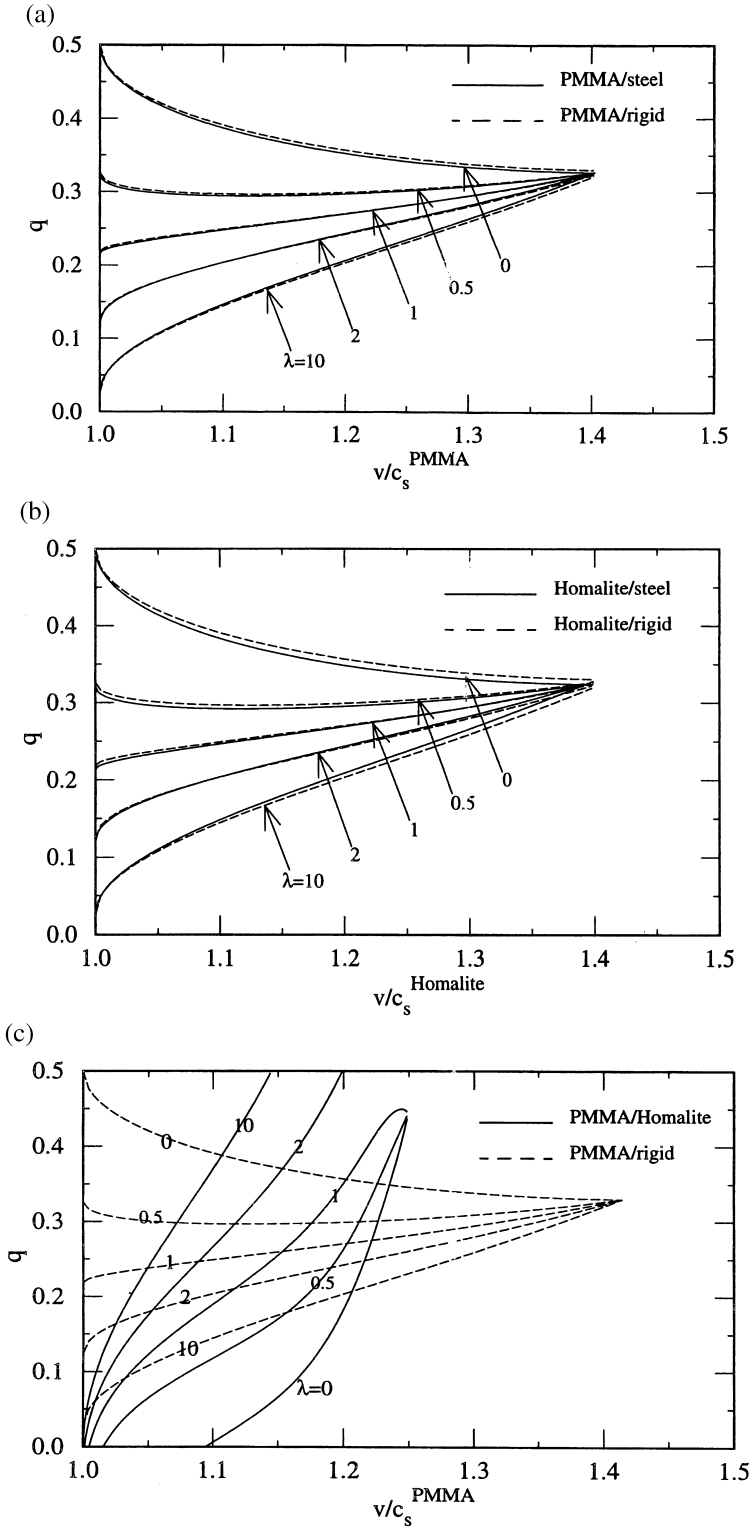

Fig. 2. The power of stress singularity q at the crack tip versus the normalized crack tip velocity, υ/c_s, under plane-stress deformation for several contact coefficients of proportionality λ, where c_s is the shear wave speed of the more compliant constituent in the bimaterial: (a) PMMA/steel bimaterial; (b) Homalite/steel bimaterial; (c) PMMA/Homalite bimaterial.

oscillatory near-tip field. Without loss of generality, three powers of stress singularity can be arranged in the order of $q_1 \geq q_2 \geq q_3$ such that q_1 is the most singular power in the near-tip stress field. For all crack tip velocities, bimaterial properties and the contact coefficients of proportionality λ, our numerical solutions of the eigenvalue problem have shown that q_2 and q_3 are identically zero. Therefore, the power of singular near-tip stress field, denoted by $q = q_1$, is given by

$$q = \frac{1}{2\pi i} \ln\left(\frac{|P| \cdot |\bar{M}|}{|\bar{P}| \cdot |M|}\right) \tag{23}$$

where $\|$ stands for the determinant of a matrix.

Fig. 2a shows the power of stress singularity q at the crack tip versus the normalized crack tip velocity, υ/c_s^{PMMA}, for PMMA/steel bimaterial under plane stress deformation. The contact coefficients of proportionality are λ = 10, 2, 1, 0.5 and 0, and c_s^{PMMA} is the shear wave speed of PMMA. This bimaterial was used in Liu et al.'s [6] and Lambros and Rosakis' [5] experiments, and the material properties are given in Table 1. The curves corresponding to the PMMA/rigid bimaterial studied by Huang et al. [4] are also shown in Fig. 2a. It is observed that the PMMA/rigid bimaterial model is an excellent approximation to the PMMA/steel bimaterial. Therefore it is reasonable for Huang et al. [4] to use the elastic/rigid bimaterial model, which has a simple, analytic full-field solution, to analyze Lambros and Rosakis' [5] experimentally obtained fringe patterns and data. Another interesting observation is that, for the PMMA/steel bimaterial, there exists a critical velocity, $1.403c_s^{PMMA}$, at which all curves coincide in Fig. 2a. Similar to the discussion of Huang et al. [4], this speed determines whether crack faces have contact for the PMMA/steel bimaterial. For crack tip speed less than $1.403c_s^{PMMA}$, there is crack face contact. Once the crack tip speed reaches $1.403c_s^{PMMA}$, crack face contact disappears and the power of stress singularity q becomes independent of the contact coefficient of proportionality λ, as evidenced by all curves for PMMA/steel bimaterial coincide at the speed of $1.403c_s^{PMMA}$. The crack faces remain traction-free as the crack tip speed exceeds $1.403c_s^{PMMA}$.

Fig. 2b shows a similar plot for the Homalite/steel bimaterial, where Homalite was used in Singh et al.'s [8] experiments, and its material properties can be found in Table 1. Curves corresponding to the Homalite/rigid bimaterial are also shown. It is confirmed that the elastic/rigid model is also an excellent approximation to the Homalite/steel bimaterial. The critical

Table 1
Material properties and wave speeds of selected materials

	Shear modulus μ (GPa)	Poisson's ratio ν	Density ρ (kg/m^3)	Shear wave speed c_s (m/s)	Plane stress longitudinal wave speed c_1 (m/s)
PMMA	1.2	0.35	1190	1004	2090
AISI 4340 steel	80.0	0.30	7833	3196	5979
Homalite-100	1.96	0.35	1230	1255	2203

crack tip speed that governs the crack face contact is $1.399c_s^{\text{Homalite}}$, where all curves for Homalite/steel coincide in Fig. 2b.

It should be pointed out, however, that the elastic/rigid model is a good approximation only to bimaterials that have a relatively large elastic mismatch, such as PMMA/steel and Homalite/steel. Fig. 2c shows the power of stress singularity q at the crack tip versus the normalized crack tip velocity, $\upsilon/c_s^{\text{PMMA}}$, for PMMA/Homalite bimaterial. Curves corresponding to an elastic/rigid model are also presented for comparison. It is clearly observed that the two sets of curves corresponding to elastic/elastic and elastic/rigid models are far apart, because the elastic modulus of Homalite is only 70% higher than that of PMMA. Accordingly, the elastic/rigid model is not applicable.

4. Asymptotic field near the trailing end of the contact zone

The asymptotic field near the trailing end of the contact zone is investigated in this section for a crack propagation intersonically along a bimaterial interface. A local coordinate system (ζ_1, ζ_2) centered at the trailing end of the contact zone is used, where (ζ_1, ζ_2) is related to the coordinate (η_1, η_2) centered at the propagating crack tip by $\zeta_1 = \eta_1 + l$, $\zeta_2 = \eta_2$, and l is the length of the contact zone. It is noted that $\zeta_1 > 0$ and $\zeta_1 < 0$ correspond to the contact zone and traction-free crack face, respectively.

The contact conditions in Eqs. (12) and (13) still hold except that $\eta_i (i = 1,2)$ are replaced by $\zeta_i (i = 1,2)$ and $\eta_1 < 0$ is replaced by $\zeta_1 > 0$. Accordingly, Eq. (15) also holds in the contact zone, i.e.

$$P\begin{bmatrix} F_1''^{+}(\zeta_1) \\ \bar{F}_2''^{+}(\zeta_1) \\ \bar{G}_2''^{+}(\zeta_1) \end{bmatrix} - \bar{P}\begin{bmatrix} \bar{F}_1''^{-}(\zeta_1) \\ F_2''^{-}(\zeta_1) \\ G_2''^{-}(\zeta_1) \end{bmatrix} = 0 \qquad \zeta_1 > 0 \tag{24}$$

where the matrix P is given in Eq. (16). Based on analytical continuation, Eq. (24) defines the following analytic function $\vec{\boldsymbol{\Theta}}'(\tilde{z})$

$$\left.\begin{aligned} \vec{\Theta}'(\tilde{z}) &= P\begin{bmatrix} F_1''(\tilde{z}) \\ \bar{F}_2''(\tilde{z}) \\ \bar{G}_2''(\tilde{z}) \end{bmatrix} \quad \operatorname{Im}(\tilde{z}) \geq 0 \\ \vec{\Theta}'(\tilde{z}) &= \bar{P}\begin{bmatrix} \bar{F}_1''(\tilde{z}) \\ F_2''(\tilde{z}) \\ G_2''(\tilde{z}) \end{bmatrix} \quad \operatorname{Im}(\tilde{z}) < 0 \end{aligned}\right\} \tag{25}$$

where $\tilde{z} = \zeta_1 + i\zeta_2$ and $\vec{\boldsymbol{\Theta}}'(\tilde{z})$ is analytic in the entire $\tilde{z}$-plane, except on the traction-free crack face ($\zeta_2 = 0$, $\zeta_1 < 0$).

The traction-free boundary conditions on the crack face outside the contact zone give

$$\sigma_{12}^{(1)} = 0 \tag{26a}$$

$$\sigma_{22}^{(1)} = 0 \tag{26b}$$

$$\sigma_{12}^{(2)} = 0 \tag{26c}$$

$$\sigma_{22}^{(2)} = 0 \tag{26d}$$

and

$$\zeta_1 < 0 \tag{26e}$$

The substitution of stresses in Eq. (7) into the above traction-free conditions and elimination of function g give [3, 4]

$$Q\begin{bmatrix} F_1''^{+}(\zeta_1) \\ \bar{F}_2''^{+}(\zeta_1) \\ \bar{G}_2''^{+}(\zeta_1) \end{bmatrix} - \bar{Q}\begin{bmatrix} \bar{F}_1''^{-}(\zeta_1) \\ F_2''^{-}(\zeta_1) \\ G_2''^{-}(\zeta_1) \end{bmatrix} = 0 \qquad \zeta_1 < 0 \tag{27}$$

where

$$Q = \begin{bmatrix} 4\hat{\alpha}_{s1}\alpha_{l1} - i(1-\hat{\alpha}_{s1}^2)^2 & 0 & 0 \\ 0 & -i(1+\alpha_{s2}^2) & -2i\alpha_{s2} \\ 0 & 2\alpha_{l2} & 1+\alpha_{s2}^2 \end{bmatrix} \tag{28}$$

In terms of the analytic function $\boldsymbol{\Theta}'(\tilde{z})$ in Eq. (25), Eq. (27) can be expressed as

$$QP^{-1}\vec{\Theta}'^{+}(\zeta_1) - \bar{Q}\bar{P}^{-1}\vec{\Theta}'^{-}(\zeta_1) = 0 \qquad \zeta_1 < 0 \tag{29}$$

Let λ_1^*, λ_2^* and λ_3^* be eigenvalues and $\vec{\boldsymbol{\chi}}_1^*$, $\vec{\boldsymbol{\chi}}_2^*$ and $\vec{\boldsymbol{\chi}}_3^*$ be the corresponding orthogonal eigenvectors for the following auxiliary eigenvalue problem

$$QP^{-1}\vec{\chi}^* - \lambda^*\bar{Q}\bar{P}^{-1}\vec{\chi}^* = 0 \tag{30}$$

which can be easily solved by a numerical method. The function $\vec{\boldsymbol{\Theta}}'(\tilde{z})$ is written in terms of eigenvectors $\vec{\boldsymbol{\chi}}_i^*$ (i = 1,2,3) as

$$\vec{\Theta}'(\tilde{z}) = \left(\vec{\chi}_1^*, \vec{\chi}_2^*, \vec{\chi}_3^*\right)\left[\xi'_1(\tilde{z}), \xi'_2(\tilde{z}), \xi'_3(\tilde{z})\right]^{\mathrm{T}} \tag{31}$$

where $\xi'_{\mathrm{i}}{}_{\mathrm{i}}(\tilde{z})$ (i = 1,2,3) are analytic except at the crack face. The substitution of expansion (31) into Eq. (29) gives

$$\begin{bmatrix} \lambda_1^* \xi_1'^+(\zeta_1) - \xi_1'^-(\zeta_1) \\ \lambda_2^* \xi_2'^+(\zeta_1) - \xi_2'^-(\zeta_1) \\ \lambda_3^* \xi_3'^+(\zeta_1) - \xi_3'^-(\zeta_1) \end{bmatrix} = 0 \qquad \zeta_1 < 0 \tag{32}$$

which constitutes three Riemann–Hilbert problems for $\xi_1'(\tilde{z})$, $\xi_2'(\tilde{z})$ and $\xi_3'(\tilde{z})$, respectively. Their general solutions are

$$\xi_j'(\tilde{z}) = B_j(\tilde{z})/\tilde{z}^{p_j} \qquad j = 1, 2, 3 \tag{33}$$

where $B_j(\tilde{z})$ are analytic functions in the entire $\tilde{z}$-plane, and p_j are the powers of stress singularity at the trailing end of contact zone and are given by

$$p_j = \frac{1}{2\pi i} \ln \lambda_j^* \qquad j = 1, 2, 3 \tag{34}$$

These powers of stress singularity p_j depend on the crack tip velocity υ, bimaterial properties, as well as the contact coefficient of proportionality λ. In fact, they are always real and two of them are identically zero, namely $p_2 = p_3 = 0$. Therefore, the non-vanishing power of stress singularity $p = p_1$ at the trailing end of contact zone is given by

$$p = \frac{1}{2\pi i} \ln \left(\frac{|Q| \cdot |\bar{P}|}{|\bar{Q}| \cdot |P|} \right) \tag{35}$$

where $\|$ stands for the determinant of a matrix.

From Eqs. (23) and (35), the sum of powers of stress singularity at the crack tip and at the trailing end of the contact zone, $p + q$, is given by

$$p + q = \frac{1}{2\pi i} \ln \left(\frac{|Q| \cdot |\bar{M}|}{|\bar{Q}| \cdot |M|} \right) \tag{36}$$

It is observed that $p + q$ is independent of the contact coefficient of proportionality λ because the matrix M is obtained from the continuity conditions across the interface and Q is derived from the traction-free crack faces, i.e. matrices M and Q do not involve the contact coefficient of proportionality λ.

Fig. 3a–c shows the power of stress singularity p at the trailing end of the contact zone versus the normalized crack tip velocity $\upsilon/c_s^{\mathrm{PMMA}}$ for PMMA/steel, Homalite/steel and PMMA/Homalite bimaterials, respectively. The corresponding power p estimated from an elastic/rigid model [4] is also shown for comparison. It is clearly observed that the elastic/rigid model is an excellent approximation to the PMMA/steel and Homalite/steel bimaterials. All curves for PMMA/steel in Fig. 3a and for Homalite/steel in Fig. 3b coincide at the same crack tip speeds as those in Fig. 2a and 2b, $1.403c_s^{\mathrm{PMMA}}$ and $1.399c_s^{\mathrm{Homalite}}$, respectively. This confirms the critical crack tip speed governing the crack face contact. However, curves in Fig. 3c for PMMA/Homalite are far away from those for an elastic/rigid model because of the relatively small elastic mismatch.

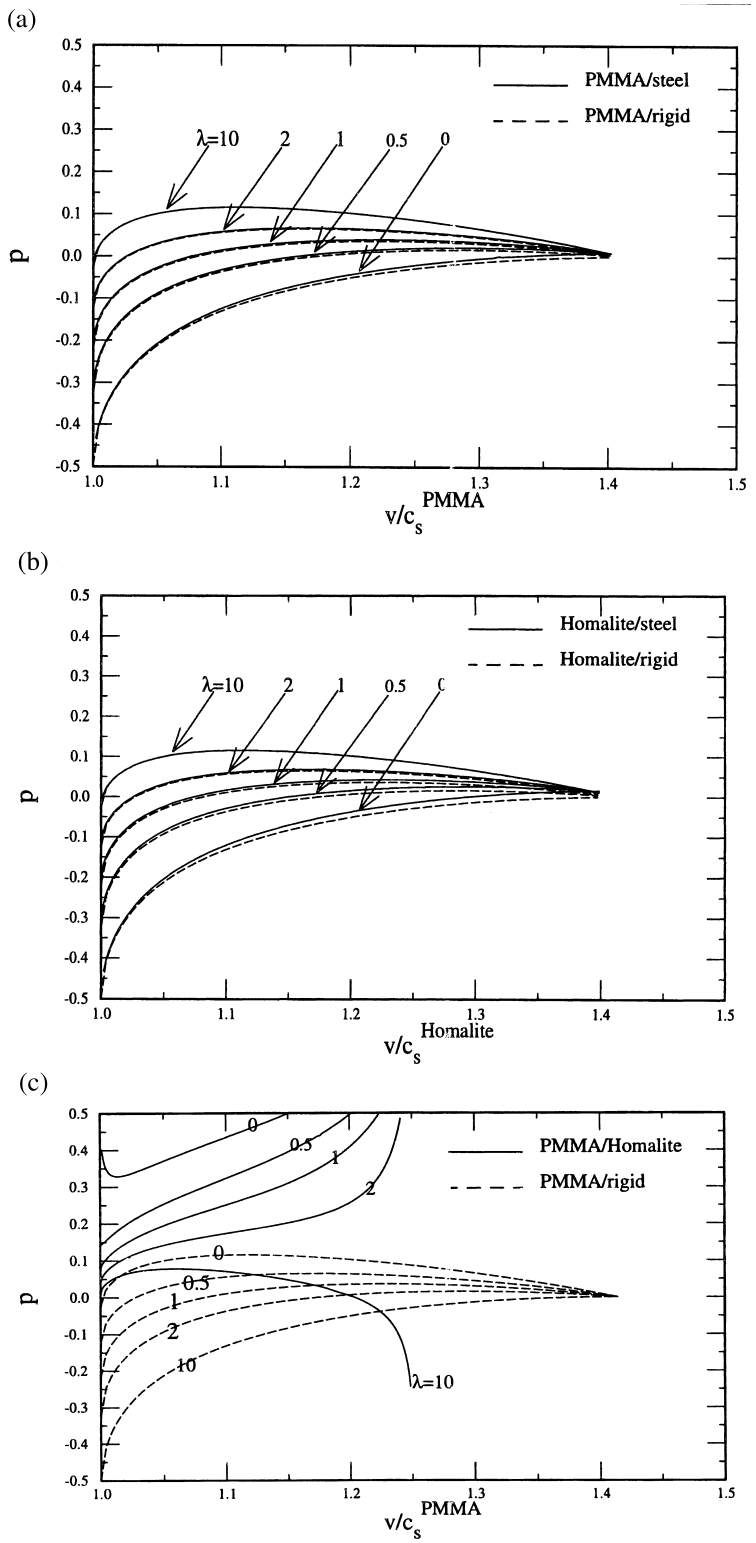

Fig. 3. The power of stress singularity p at the trailing end of the contact zone versus the normalized crack tip velocity, v/c_s, under plane-stress deformation for several contact coefficients of proportionality λ, where c_s is the shear wave speed of the more compliant constituent in the bimaterial: (a) PMMA/steel bimaterial; (b) Homalite/steel bimaterial; (c) PMMA/Homalite bimaterial.

5. Conclusions

The asymptotic fields near the crack tip and near the trailing end of the contact zone are obtained for a crack propagating intersonically along a bimaterial interface with crack face contact. It is established that, for a bimaterial with relatively large elastic mismatch between its constituents, an elastic/rigid model is a reasonable approximation for the elastic/elastic bimaterial, regardless of their mismatch in mass densities. Therefore, for all experiments on intersonic crack growth that are presently available, e.g. PMMA/steel [5] and Homalite/steel [8], the elastic/rigid model provides a useful means for analyzing the experimental fringe patterns and data. The is because the elastic/rigid model gives a simple, analytic full-field solution [4], while no closed-form solutions have been established for the elastic/elastic bimaterial. The asymptotic analyses near the crack tip and near the trailing end of the contact zone have confirmed the existence of a critical crack tip speed below which crack face contact occurs.

Acknowledgements

Y.H. gratefully acknowledges the support from National Science Foundation (grant no. INT-94-23964, CMS 96-10491, DMI 96-10454), Motorola Foundation and Ford Foundation. A.J.R. acknowledges the support from ONR (grant no. N00014-95-1-0453) and NSF (grant no. MSS-90-24838).

References

[1] Atkinson C. Dynamic crack problems in dissimilar media. Mech Fracture 1997;4:213–48.
[2] Freund LB. Dynamic fracture mechanics. Cambridge: Cambridge University Press, 1990.
[3] Huang Y, Liu C, Rosakis AJ. Transonic crack growth along a bimaterial interface: an investigation of the asymptotic structure of near-tip fields. Int J Solids Structures 1996;33(18):2625–45.
[4] Huang Y, Wang W, Liu C, Rosakis AJ. Intersonic crack growth in bimaterial interfaces: an investigation of crack face contact. J Mech Phys Solids (in;(press)):.
[5] Lambros J, Rosakis AJ. Shear dominated transonic crack growth in a bimaterial—I. Experimental observations. J Mech Phys Solids 1995;43(2):169–88.
[6] Liu C, Lambros J, Rosakis AJ. Highly transient elasto–dynamic crack growth in a bimaterial interface: higher order asymptotic analysis and optical experiment. J Mech Phys Solids 1993;41(12):1887–954.
[7] Liu C, Huang Y, Rosakis AJ. Shear dominated transonic crack growth in a bimaterial—II. Asymptotic fields and favorable velocity regimes. J Mech Phys Solids 1995;43(2):189–206.
[8] Singh RP, Lambros J, Shukla A, Rosakis AJ. Investigation of the mechanics of intersonic crack propagation along a bimaterial interface using coherent gradient sensing and photoelasticity. Proc R Soc Lond (in;(press)):.
[9] Tippur HV, Rosakis AJ. Quasi-static and dynamic crack growth along bimaterial interfaces: a note on crack-tip field measurement using coherent gradient sensing. Expl Mech 1991;31(3):243–51.
[10] Xu X-P, Needleman A. Numerical simulations of dynamic crack growth along an interface. Int J Fracture 1996;74:289–324.
[11] Yang W, Suo Z, Shih CF. Mechanics of dynamic debonding. Proc R Soc Lond 1991;A433:679–97.
[12] Yu H, Yang W. Mechanics of transonic debonding of a bimaterial interface: the in-plane case. J Mech Phys Solids 1995;43:207–32.